Photocatalytic activity of twist-angle stacked 2D TaS$_2$

Evgeniya Kovalska*, Pradip Kumar Roy, Nikolas Antonatos, Vlastimil Mazanek, Martin Vesely,

Bing Wu, Zdenek Sofer*

University of Chemistry and Technology Prague, Technická 5, 166 28 Prague 6, Czech Republic

ABSTRACT: The development of low-cost efficient photoelectrosensitive electrodes as an alternative to the expensive and complex rigid systems is yet in huge demand for advanced photoresponsive technology. Herein, the light-induced efficiency of electrochemically exfoliated TaS$_2$ nanosheets for hydrogen generation catalysis and photodetectors has been demonstrated for the first time. The electrochemical exfoliation of TaS$_2$ crystals toward a few-layer derivative has been pioneered in anhydrous tetrabutylammonium hexafluorophosphate in N, N-dimethylformamide. Comprehensive analysis of as-exfoliated TaS$_2$ revealed the formation of nanoparticles and nanosheets with a lateral size of about several nanometers and micrometers, correspondingly. Observed mutual twisting of 2H-TaS$_2$ flakes leads to the redistribution of charge density induced by interlayer interaction of the individual nanosheets. External light irradiation on the TaS$_2$ surface influences its conductivity making the material feasible for photoelectrocatalysis and photodetection. The TaS$_2$-based catalyst demonstrates high HER photoelectrocatalytic activity with the onset overpotential below 575 mV vs. RHE which can be lowered by thorough catalyst preparation. Finally, the TaS$_2$-integrated photodetector in the acidic medium represents its broadband light sensing capability with the highest photoresponsivity (0.68 mA W^{-1}) toward 420

nm light illumination. This finding will pave the way to a new realization of exfoliated twist-angle stacked TaS_2 for photo-induced electrochemistry and sensing.

INTRODUCTION

With increasing demands in modern society, the energy crisis and environmental problems are currently on the spotlight. Hydrogen is found to be the main sustainable source for renewable energy and is highly required for advanced energy conversion systems. Recently, photoelectrocatalytic and photoelectrochemical water-splitting methods are found as an efficient approach for the scalable generation of hydrogen. The concept of light-induced energy production through semiconductor catalysts attracted many research efforts aiming at the development of low-cost efficient bifunctional materials for hydrogen production and environment-sensing response. The performance of these materials can be tuned while illuminating the light of various wavelengths. The occurred photo-induced electron transfer in the targeted nanosheets-based sensitive material, will generate photoelectrochemical water-splitting *e.g.* faster hydrogen evolution reaction (HER) or broadband light-sensitive detector. These will pave new ways for emerging materials as a cheaper and more productive alternative to most common fossil fuels-based methods of hydrogen production as well as traditional photodetectors.

Two-dimensional (2D) transition-metal dichalcogenides (TMDs) have been demonstrated as promising catalysts for water splitting, hydrogen reduction and water oxidation.[1, 2] The unique chemical and physical properties of 2D TMDs are demonstrated by their small size enriched by the number of edge active sites, band-edge position, quantum confinement effect and thus, exhibit photo-induced catalytic efficiency.[3] TMDs are considered as the most promising cost-effective catalysts and their properties are determined by the TMDs' polymorph type namely hexagonal 2H

or trigonal 1T. It has been reported that stable 2H-MoS$_2$ shows semiconducting properties meanwhile metastable 1T-MoS$_2$[4] or 1T-WS$_2$[5] forms demonstrate metallic properties. The metallic phase of a material is capable of a more efficient performance than the semiconducting 2H counterpart owing to its enhanced electrical conductivity. The metallic character is associated with undercoordinated chalcogen atoms at the 1010 edge of 2D TMD providing for instance more efficient adsorption of hydrogen which is a crucial step for electrochemical water splitting[6]. The MoS$_2$ and WS$_2$ exhibit superior catalytic activity and are used as alternatives to Pt-based catalysts[7-9]. The WSe$_2$ is demonstrated as an excellent output stability photodetector due to its high absorption coefficient in the visible and near-infrared regions[10, 11]. Other known 2D materials such as TiSe$_2$,[12-14] NiSe$_2$,[15, 16] TaSe$_2$[17] and TaS$_2$[18-20] are interesting due to their superconductivity, charge-density-wave and metal-insulator transitions.

Among other 2D TMD materials, tantalum disulfide (TaS$_2$) has been subject to numerous studies due to the variety of the material's unique structural and electronic phases.[21] Its initial metallicity and thus, electrical conductivity can lead to potential applications such as a light-responsive active electrode in the HER and photosensing. Albeit, the study of TaS$_2$ is mainly focused on the superconductivity,[22-24] field emission[25, 26], meanwhile, photo-induced features of the material for HER and photosensing have not been explored yet. Aiming to enhance the photoresponse performance of the TaS$_2$, the quality and dimensions of the material must be considered. For instance, bulk TaS$_2$ possesses a lack of exposed active sites that significantly affect the conversion efficiency of the material and narrows its application. Therefore, a thorough cleavage of the van der Waals structure by selecting the most appropriate method is essential to increase the conversion efficiency of TaS$_2$.

Several methods have been demonstrated to produce layered TaS_2 such as chemical vapor deposition (CVD),[27] mechanical cleavages,[28] intercalation,[29] ultrasonication[30-32], or liquid-phase exfoliation.[22] However, the CVD method remains to be improved before it can be used to produce large-domain homogeneous TaS_2 films. The mechanical cleavage is not scalable and undergoes a lack of control over product thickness and size. Alternatively, electrochemical exfoliation (one of the solution-based techniques) is the most convenient, simple and controlled method that can be employed in ambient temperature for large-scale production of 2D TaS_2. Recently the electrochemical approach has been successfully applied for the exfoliation of a few-layer phosphorene[33] and arsenene[34] and has been pioneered for single-step production of platinoid-decorated phosphorene.[35]

Therefore, in this study, the photoresponse of electrochemically exfoliated TaS_2 nanosheets and preliminarily characterized by micro- and spectroscopic techniques (Supporting Information: N1) was investigated in an effort to develop a low-cost efficient photosensitive electrode that can replace the noble metal-based catalysts[36] (as photoelectrocatalyst – PEC) and CMOS-based photodetectors[37] (as photodetector – PD). Pioneered low-potential electrochemical exfoliation of TaS_2 crystals was carried out in the non-aqueous electrolyte medium of tetrabutylammonium hexafluorophosphate (TBAPF$_6$) in N, N-dimethylformamide (DMF). The as-exfoliated 2D TaS_2 nanostructures consist of the few-layer nanosheets and nanoparticles. Detailed characterization of bulk and exfoliated TaS_2 was performed through various microscopic and spectroscopic techniques. The photo-induced high HER electrocatalytic activity of the as-exfoliated TaS_2 nanostructures with low overpotential (> 575 mV and 320mV) was reported. A room-temperature TaS_2-based broadband photodetector in the acidic medium of 0.5 M H_2SO_4 has been presented. The higher electrical conductivity of 2D TaS_2 compared to its bulk form can improve the efficiency

of charge distribution in the catalytic/sensing systems and, thus, broaden the material's application area.
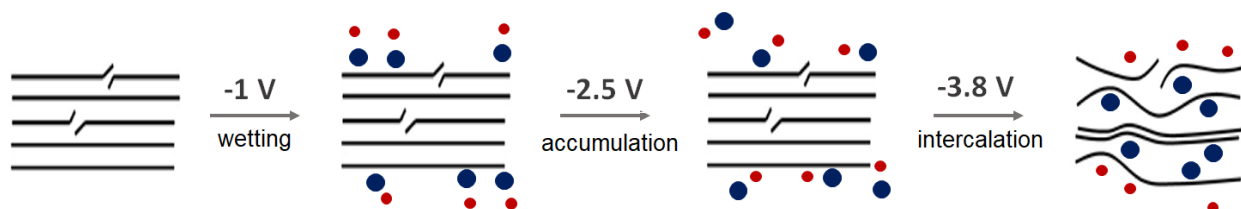
RESULTS

(I) Synthesis and characterization of the materials

Electrochemical exfoliation of bulk TaS_2 crystal (see scanning electron microscopy (SEM) images in Figures S1 a-c) was performed in the anhydrous electrolyte of 0.01 M $TBAPF_6$ in DMF. Following three main steps of the procedure (Scheme 1) namely wetting of the crystal, accumulation (or activation) of the tetrabutylammonium cations (TBA^+) and their intercalation between TaS_2 layers were carried out at -1, -2.5 and -3.8 V (vs. 0.1 M $Ag/AgNO_3$), respectively. The first two steps were completed in 2 min each, followed by 4 hours of TBA^+-assisted intercalation-delamination process at a potential of -3.8V. It has to be noted that the duration of the process is defined by the initial size of the TaS_2 crystal and can be terminated when a sufficient amount of the exfoliated material is produced.

After the exfoliation of the TaS_2 crystal, flakes of various sizes and thicknesses were observed based on AFM analysis. These include TaS_2 nanosheets of lateral size up to 6 μm with a thickness of 30 nm as well as 2.3 μm nanosheets with 7 nm thickness. (Figure 1 a, b respectively). In addition, recognized TaS_2 nanoparticles demonstrated a lateral size of 100-200 nm and thickness in the range between 0.5 – 3 nm. (Figure 1 c). The successful exfoliation of the TaS_2 crystal into nanosheets and nanoparticles as well as their size distribution were confirmed by the statistical analysis (Figure 2) obtained from AFM images. The results are also in good agreement with STEM images (Figures S1d-f) as well as TEM images coupled with EDX (Figure S2) where

the dispersion of two-types of exfoliated nanostructures with the lateral size of about tens and hundreds of nanometers as well as several micrometers are depicted.

Scheme 1. Electrochemical exfoliation of TaS_2 crystal*

*Blue ● – cations (TBA^+); red ● – anions (PF^-_6).

TEM and SAED microscopies demonstrate good quality of exfoliated TaS_2 nanosheets (Figure 3 a-d) of hexagonal structure (schematic image, Figure 3 e, f). High-resolution TEM images in Figure S3 also show the formation of round-shaped TaS_2 nanoparticles that are localized on the surface of the larger flakes. This is consistent with the statistical analysis of particle size distribution (Figure 2) that confirms the production of two types of TaS_2 nanostructures. Based on the fast Fourier transform (FFT) analysis of TEM images (Figure S4), the crystal symmetry of TaS_2 is demonstrated as the fringes oriented in a three-fold rotation axis. The d-spacing of the symmetry of the TaS_2 crystal of about 2.9 Å and 2.93 Å defines its (100) planes' orientations. The electron diffraction patterns of a flat area of the TaS_2 nanosheet show this growing direction. Different magnification TEM images of the TaS_2 exhibit in-plane atoms ordering with the lattice spacing 0.305 nm. The morphology of the exfoliated material and thus sharply defined layered appearance are caused by the initial structure of the TaS_2 crystal.
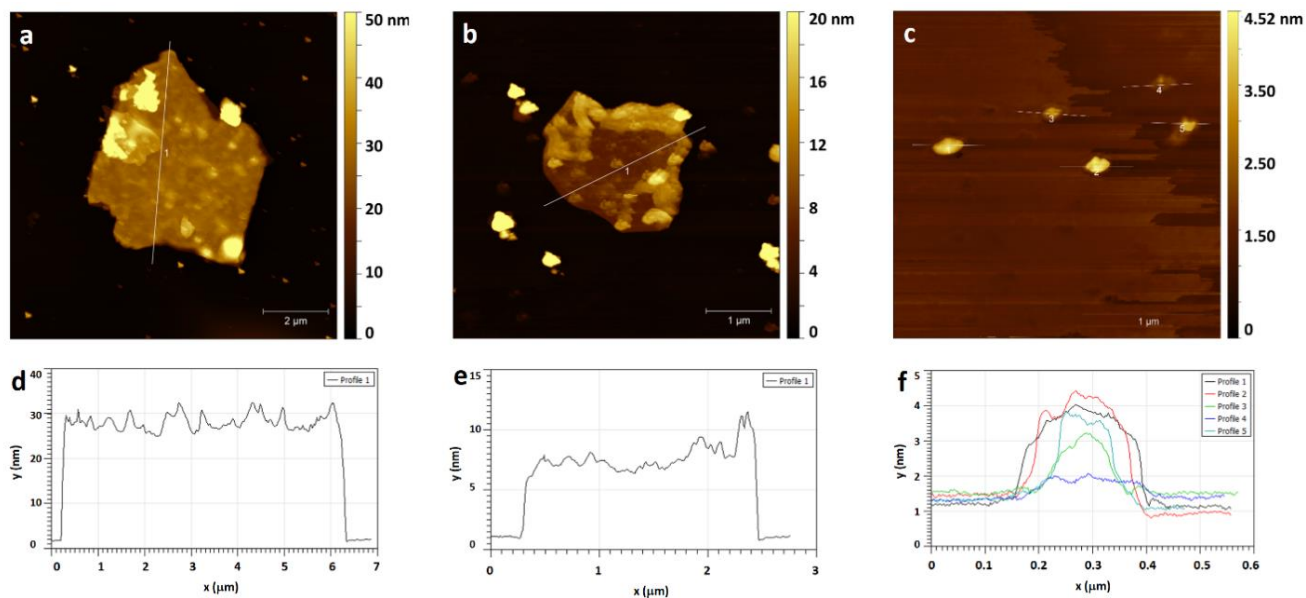
Figure 1. AFM images of the as-exfoliated TaS_2 nanosheets (a, b), nanoparticles (c) and their corresponding height profiles (d-f).
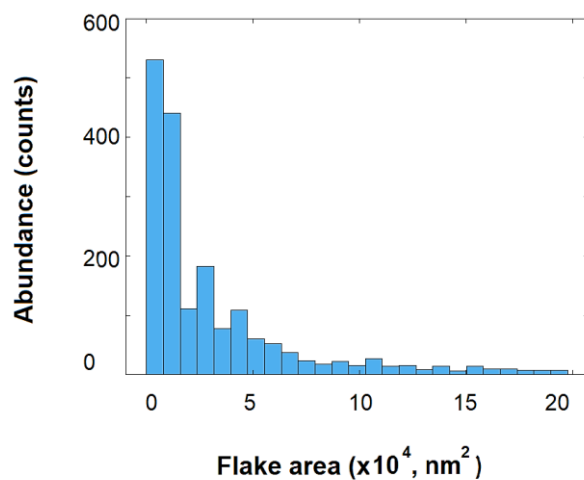

Figure 2. The statistical analysis of the particle size distribution of exfoliated TaS_2 in DMF. The evaluation was conducted based on the AFM results.
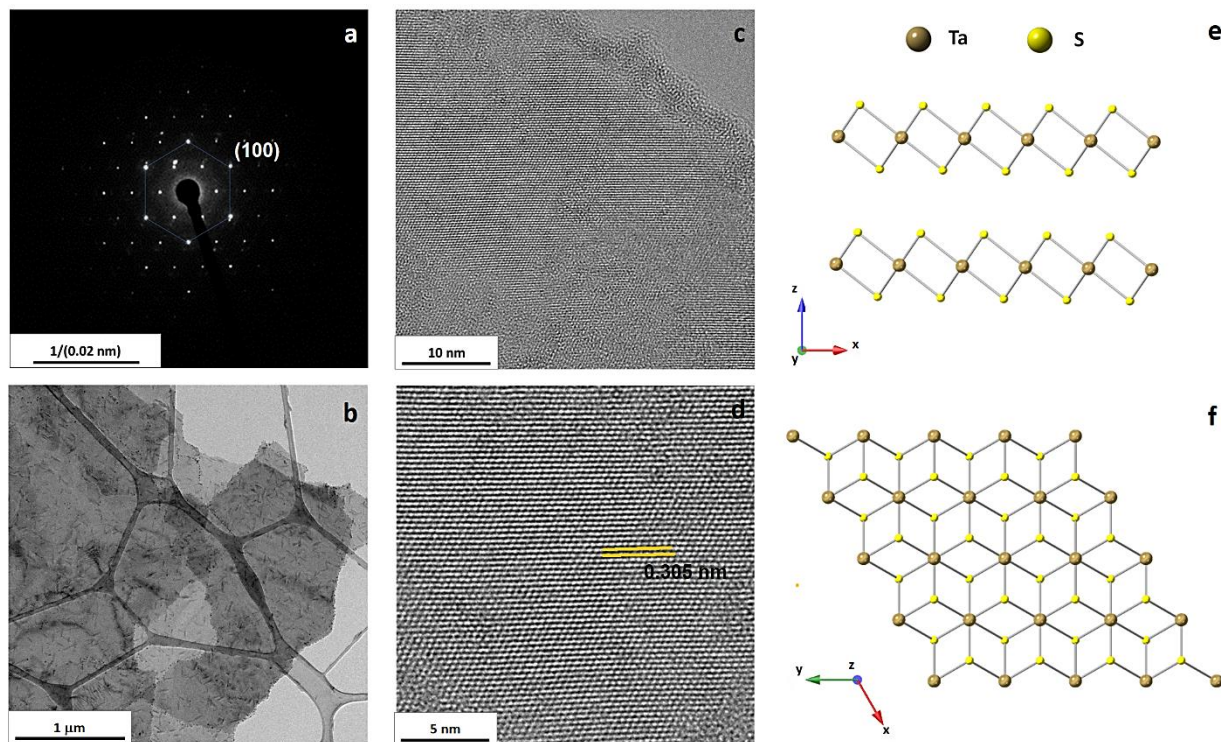
Figure 3. Morphological and structural analysis of electrochemically exfoliated TaS_2. (a) SAED pattern; (b) low-resolution TEM image; (c, d) high-resolution TEM images; schematic (e) side and (f) top views of the TaS_2 structure.

The SAED patterns of the large area TaS_2 flakes (Figure S5) verified several configurations with their different twist angles of 7°, 8°, 9°, 10° (Figure 4). The trigonal arrangement of Ta atoms in Figure 3 e, f corresponds to the standard stacking of S-Ta-S in the unit cell. This direct stacking of each layer via Ta atoms was experimentally and theoretically proven in a few publications.[38-40] The increase of both formation energy and bandgap has been theoretically explained due to the interlayer interaction of twisted TaS_2 flakes and the redistribution of charge density induced by the in-plane distortion.[39] This feature can also lead to the increase of the electronic specific-heat coefficient of the randomly twisted TaS_2 nanosheets[22] establishing the material as a promising candidate for photo-induced applications.[41]
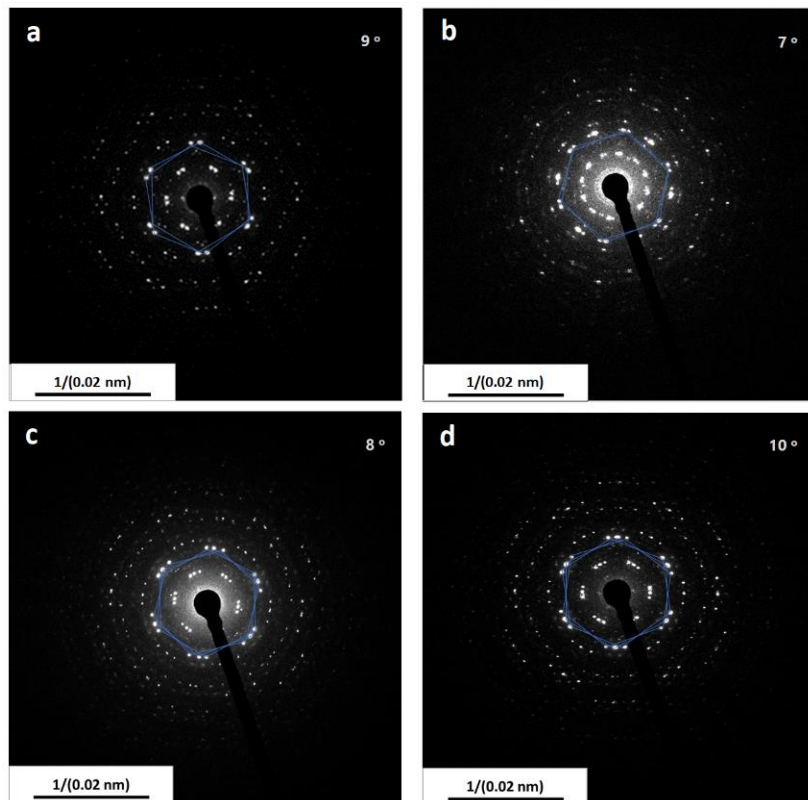
Figure 4. The SAED patterns are taken from a large area that refers to the various twist of the (a, b) bilayer and (c, d) three-layer TaS$_2$.

The analysis of the crystal structure and optical characteristics of the bulk and exfoliated TaS$_2$ is demonstrated in Figure 5. X-ray diffraction (XRD) was used to verify the successful synthesis of hexagonal 2H-TaS$_2$ (Supporting Information: N2, 3). The XRD pattern in Figure 5 a confirmed the *P-3m1* hexagonal structure of TaS$_2$ (PDF: 04-003-4190). No other phases were observed indicating the purity of the starting material. The sharp peaks in the pattern ascertaining the high crystallinity of the sample. Similar peaks were observed in the exfoliated material's XRD pattern albeit broadened and with lower intensity caused by the disruption of initial crystallinity due to the exfoliation procedure. The broadening of the XRD peaks is an indication of a decrease in crystal size and lattice strain increase. Figure 5 b shows the Raman spectra of bulk and as-exfoliated TaS$_2$ samples. Three main Raman features depicted at 239, 301 and 373 cm^{-1} from the

bulk crystal were assigned to the E_{2g}, E_{1g} and A_{1g} modes respectively.[29, 42] More prominent peaks of the same modes and their 4 cm^{-1} redshifts were observed for the exfoliated nanosheets. The shift is attributed to the decrease of the interlayer van der Waals forces and due to the material's thickness reduction. UV-VIS absorption spectrum of the as-exfoliated TaS_2 nanostructures recorded at room temperature is demonstrated in Figure 5 c. The TaS_2 represents low in-plain reflectivity at high energies (from 400–720 nm) and vice versa at low energies accordingly.[43]
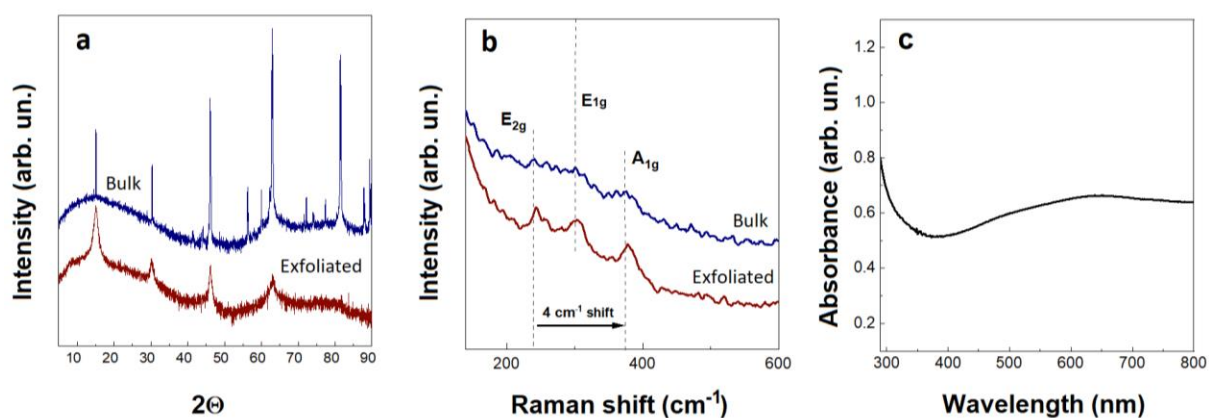

Figure 5. Structural and optical characteristics of the TaS_2: (a) XRD diffractogram of bulk TaS_2 and electrochemically exfoliated nanosheets; (b) Raman spectra of bulk and electrochemically exfoliated TaS_2; (c) UV-VIS absorbance spectra of the exfoliated TaS_2 in the DMF.

To confirm chemical composition and binding states, we have measured the survey (Figure S6) and high-resolution X-ray photoelectron spectra (HR-XPS) of Ta 4f and S 2p (Figure 6). Survey spectra confirmed composition which was close to TaS_2 for bulk and exfoliated samples as well. Since exfoliated samples were measured on a gold substrate, Au peaks can also be seen in its survey spectrum. HR-XPS Ta 4f spectra were deconvoluted with two binding states Ta^{IV} (TaS_2) and Ta^V (Ta_2O_5) with binding energies 22.9 and 26.1 eV, respectively.[44] Although O 2s at 24.0 eV overlaps with the Ta 4f, it was not used for deconvolution because its amount was

less than 1 % due to a low relative sensitivity factor of 0.14 compared to 8.62 for Ta 4f. Each binding state in Ta 4f has spin-orbit components separated by 1.92 eV. Binding state ratios are summarized in Table S1. Bulk crystal was covered by 20 % of Ta_2O_5 and after exfoliation, this amount increased to 30 %. It has to be noted that TaS_2 is susceptible to oxidation and this ability is even higher after the exfoliation.[44] Thus, operating the material in an oxygen-free environment and storing it in the dry solvents will increase the stability of as-exfoliated TaS_2.
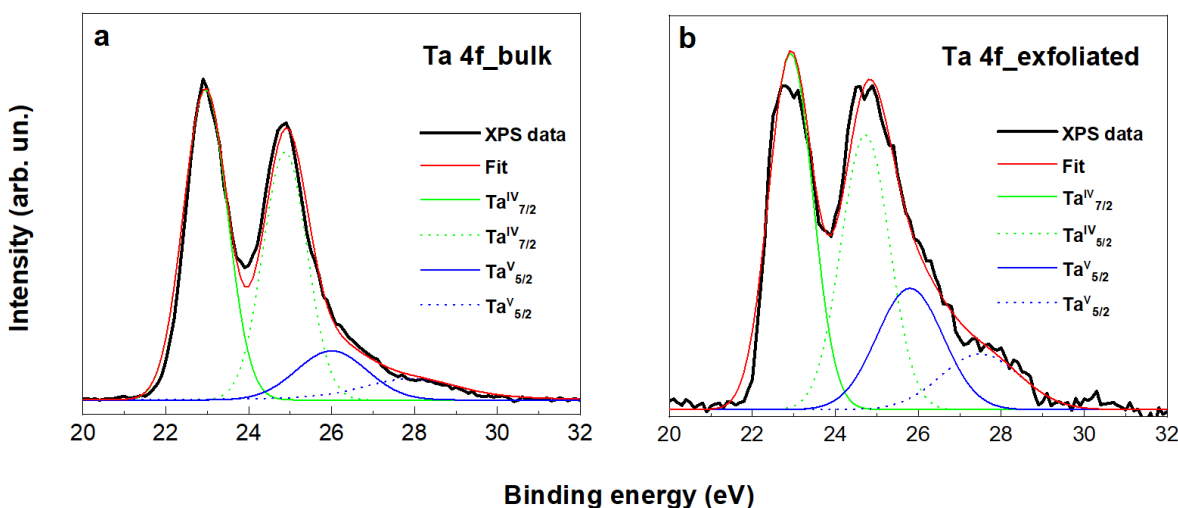

Figure 6. High-resolution XPS spectra of the (a) bulk and (b) electrochemically exfoliated TaS_2 nanostructures.

(II) Photoelectrocatalytic performance of as-exfoliated TaS_2 for HER

Light-driven electrocatalysis using semiconducting materials (*e.g.* TaS_2) or their heterostructures is one of the most promising sustainable approaches for the generation of hydrogen by water splitting.[45-47] Even though a thermal treatment or catalyst support texturization of the catalytic films is used to increase the number of active centers of the TaS_2 flakes, these methods are time-consuming and require a high-temperature and inert gas atmosphere.[48] The light-

induced electrochemistry (photoelectrochemistry) can be a simple approach to enhance the HER activity of the TaS_2. To the best of our knowledge, the photoelectrocatalytic activity of TaS_2 has not been explored to date.

Herein, the photoelectrocatalytic performance of electrochemically exfoliated TaS_2 for HER was explored for the first time (see Supporting Information: N4). The three-electrode linear sweep voltammetry (LSV) was performed in the 0.5 M H_2SO_4 employing a few-layer TaS_2 deposited on a glassy carbon as a working electrode. The measurements have been repeated in the light mode for four different wavelengths (420, 532, 630 and 720 nm). The results were compared with the dark mode for as-exfoliated TaS_2 nanosheets of mixed composition. The mixed composition consists of nanosheets of various sizes and nanoparticles as was confirmed by the STEM, AFM and statistical analysis. Few-layer TaS_2 samples of a smaller lateral size (~30-40 nm, Figure S7) were obtained as follows: first, the TaS_2 dispersion was centrifuged at 3500 rpm for 10 min; second, collected supernatant was centrifuged at 10000 rpm for 10 min and the resulting precipitate was used for the test.

As shown in Figure 7 a, b the HER for initial as-exfoliated TaS_2 starts at a potential of 575 mV (vs. RHE) under dark mode at a current density of 10 mA cm^{-2}. The overpotential under the illumination light of different wavelengths is shifting towards lower potentials, more specifically: 537, 549, 531 and 454 mV when blue, green, red and far-red light-emitting diodes (LEDs) are implemented, respectively. This behavior is attributed to the carrier increment that is generated in the TaS_2 nanosheets with light irradiation enhanced by the intrinsic defect (wrinkles) and mutual twisting of the individual layers. The current density of the TaS_2 catalyst under dark is decreased after 100 cycles (Figure S8), which demonstrates a slow degradation of the as-investigated catalyst. It has to be noted that the onset overpotential for the TaS_2 catalyst based on

flakes of smaller size was significantly reduced to approximately 320 mV (Figure 7 c). Considering the influence of the light on the as-exfoliated samples, the ~100 mV decrement of the overpotential is expected that will make a few-layer TaS_2 a superior HER photoelectrocatalyst. This study on bare TaS_2 catalysts can compete with recently reported results[49] where the performance of TaS_2 was enhanced by the incorporation of conductive films[50] or thermal treatment in the H_2-environment.[48] Furthermore, thoroughly prepared catalysts under light illumination will outperform the HER activity of commercial Pt/C electrode (~40 mV) providing a cheaper alternative.
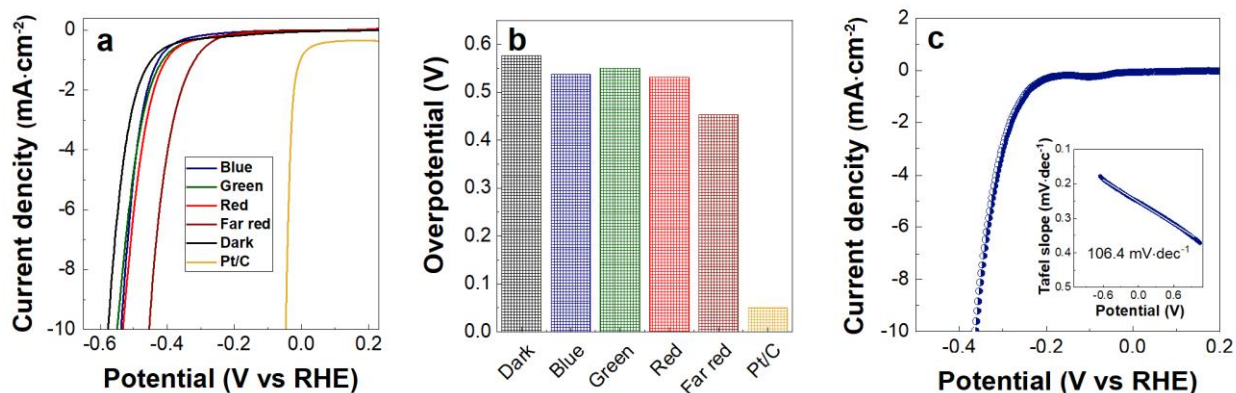

Figure 7. HER analysis in the medium of 0.5 M H_2SO_4 at the scan rate of 1 mV·s^{-1} in dark mode and during the blue, green, red and far-red irradiation. Polarization curves (a) and corresponding overpotentials (b) of exfoliated TaS_2 at a −10 mA·cm^{-2} current density; the measurements were conducted vs. RHE and compared with commercial Pt/C electrocatalyst. Polarization curve and inserted corresponding Tafel plot (c) of few-layer TaS_2 small flakes obtained after centrifugation; overpotential is 360 mV.

(III) TaS₂-integrated photodetector

Solution-based PEDs offer unique advantages over standard photodetectors in the form of a simple and easy device manufacturing process. Recently 2D nanomaterials have demonstrated their feasibility for PDs ranging from visible to THz however this is not inherent to one material.[43, 51, 52] Therefore, a broadband photodetection capability of materials is highly demanded due to its wide application possibility. The intrinsic parameters of the material's light sensitivity and response can be tuned by changing the applied voltage, analyte concentration and power of the illuminated light. Herein, the photoelectrochemical response of TaS₂ in 0.5 M H₂SO₄ acidic medium was measured in a three-electrode system at ambient temperature. The TaS₂-integrated PEC was tested under four illumination wavelengths (420, 520, 630 and 720 nm) with a scanning speed of 10 mV·s⁻¹. The procedure of photoelectrochemical measurements is described in Supporting Information: N5.

The results illustrated a steady response toward different illumination wavelengths as depicted in Figure 8. As shown in Figure 8 a, the power-dependent photocurrent measurement was achieved by using chronoamperometry in 0.5 M H₂SO₄ at 0.5 V against SCE under the illumination of 420 nm blue LED light source. The response of the TaS₂-based electrode toward blue illumination was the highest in comparison with other LEDs. The response toward green illumination (Figure 8 b) was decreased and slightly increased after applying red (Figure 8 c) and far-red (Figure 8 d) light sources. The most prominent response of the electrochemically exfoliated few-layer TaS₂ is demonstrated under blue illumination and well consistent with the light absorbance of the material (Figure 5 d). The near-linear increment in current density with the increase of the illumination power from 100 to 1200 mW was illustrated (Figure S9) for all lights.

As the intensity increases, the current response jumps to a higher value corresponding to a higher conductance, indicating that the separation of electron-hall pairs is triggered.
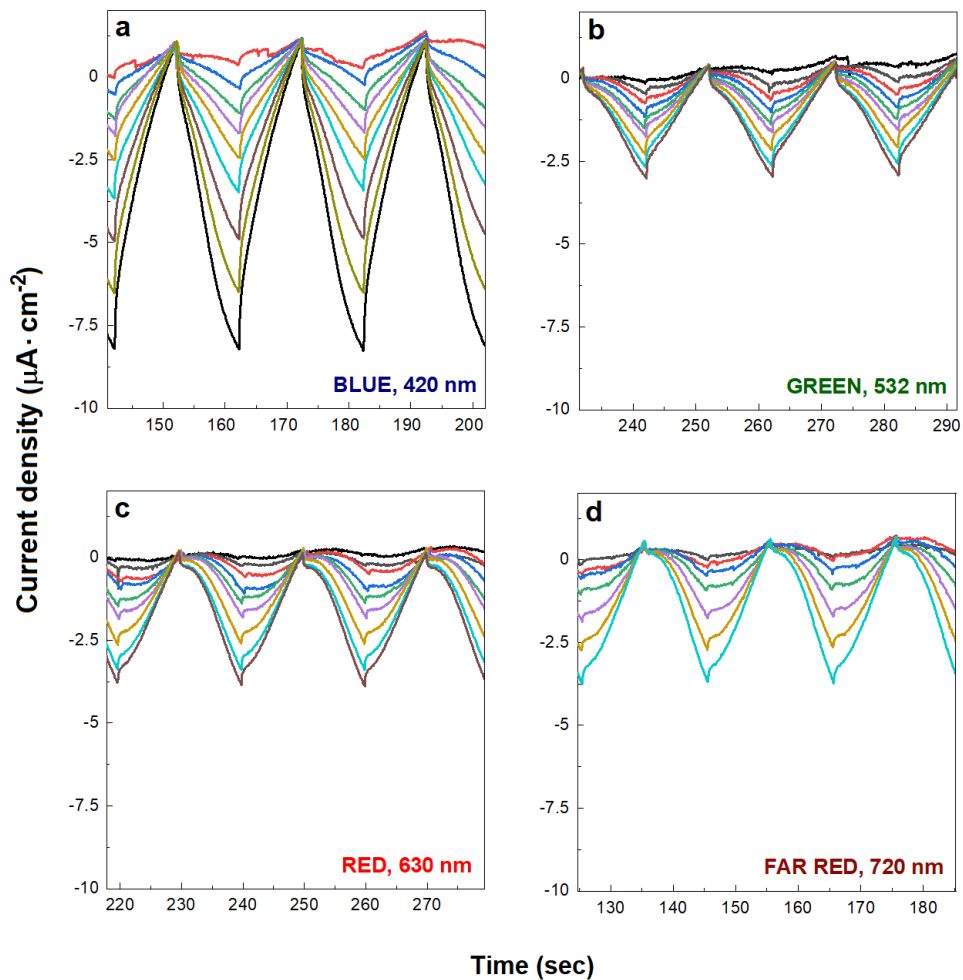

Figure 8. Power dependence of photocurrent density under the illumination of (a) blue (420 nm), (b) green (532 nm), (c) red (630 nm) and (d) far red (720 nm) LED sources in 0.5 M H_2SO_4 solution at 0.5 V vs. SCE. The power increased from 100 to 1200 mW (an arrow demonstrates the direction of power increment).

The photodetection potential of the material has been assessed in more detail by calculating a few essential parameters. At first, the photoresponsivity (R_{ph}) of the TaS$_2$-integrated PD has been calculated using the following equation: $R_{ph} = \Delta I/P$, where ΔI represents the difference in photocurrent density between the dark and photocurrent, and P is the irradiation power intensity per unit area. The calculated photoresponse demonstrated the highest responsivity of about 0.62 mA·W^{-1} under the illumination of 420 nm blue LED source at 0.5 V applied potential (vs. SCE). Figure 9a highlighted the photoresponsivity of the devices concerning the power density for different illumination wavelengths. Another important parameter for the evolution of photodetection capability is specific detectivity; it has been determined accordingly[53]

$$D^* = \frac{(AB)^{1/2}}{NEP} \qquad \text{Eq. 1.}$$

In the above equation A, B, and NEP stand for the active area, measured bandwidth, and noise equivalent power, respectively. NEP is defined as the input signal power resulting in a signal-to-noise ratio (S/R) of 1 in a 1 Hz output bandwidth. Furthermore, in the equation form, NEP can be presented as[53, 54]

$$NEP = \frac{I_N}{R_{ph}} \qquad \text{Eq. 2.}$$

Here, R_{ph} and I_N represent the photoresponsivity of the PD and the noise current, respectively. In addition, the noise, which is associated with the dark current (I_D) of the PD current, can be ascribed as $I_N^2 = 2eI_DB$, where e represents the electronic charge.[43] The calculated specific detectivity of our PD devices of about 1.28 x 10^9 cm·Hz$^{1/2}$ W^{-1} (Figure 9b).
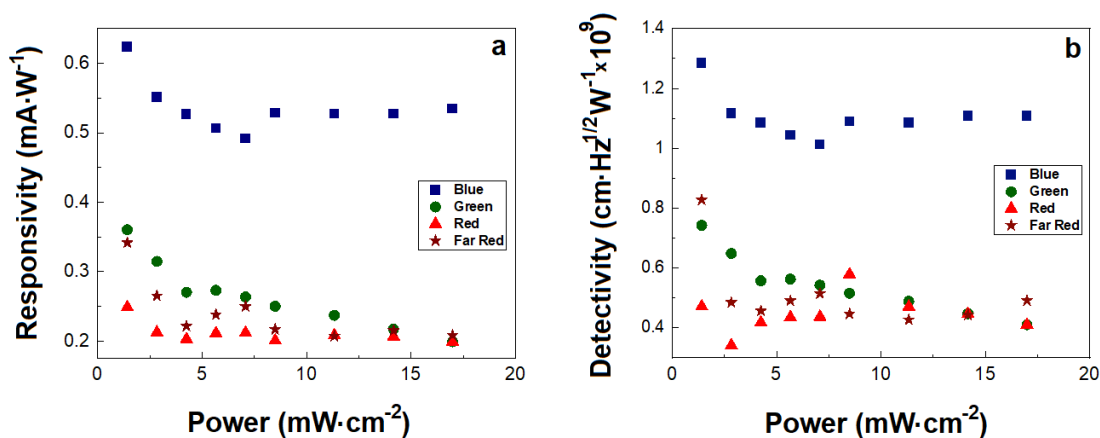
Figure 9. The responsivity (a) and specific detectivity (b) of TaS$_2$-integrated PD in 0.5 M H$_2$SO$_4$ solution as a function of power density upon four different illumination wavelengths: blue, green, red and far-red.

Prepared TaS$_2$-based PD exhibited a broadband photodetection capability with the highest photoresponsivity (0.68 mA W^{-1}) and specific detectivity (1.39 × 10^9 cm Hz$^{1/2}$ W^{-1}) toward 420 nm light illumination, which is nearly double compared with 532, 630 and 720 nm illumination wavelengths. The results demonstrate the versatility of 2H-TaS$_2$-based PEC which exhibits metal-like characteristics coupled with broadband light absorption and thus emission due to energy separated bands. The original metallicity of the TaS$_2$ that is assisted by under-coordinated atoms at edge sites is enhanced by the random twisting between the TaS$_2$ monolayers which form a rich homogeneous interface with enhanced conductivity.[22] This consequently increases the electron transfer in the "TaS$_2$ electrode/0.5M H$_2$SO$_4$ electrolyte" system and thus improves the catalytic performance of the material, establishing it favorable for electrocatalysis.[44, 1, 2]

CONCLUSIONS

The light-induced efficiency of electrochemically exfoliated TaS_2 for photoelectrocatalysis and PEC-based photodetector performance has been demonstrated for the first time. A well-controlled exfoliation process that is based on the TBA^+-cation intercalation between the TaS_2 interlayers was performed in the non-aqueous DMF medium applying a potential of-3.8 V. Few-layer TaS_2 nanosheets of different lateral sizes namely, 10-100 nm and 1–30 μm, were identified and characterized by numerous characterization and microscopy techniques. It was shown that exfoliated TaS_2 nanosheets possess a trigonal prismatic structure (2H type, hexagonal) and thus, metallic character. The metallicity of the $2H\text{-}TaS_2$ nanosheets was enhanced by the twisting of the individual flakes and their mutual interaction causing charge density redistribution. This ability was further increased by the external illumination of the light of the following wavelengths: 420 nm (blue), 532 nm (green), 630 nm (red) and 720 nm (far-red). Based on the above, TaS_2 nanosheets were tested as PEC for HER and PD of visible light. The as-exfoliated TaS_2-based catalyst under light illumination demonstrated high HER catalytic activity with the overpotential for 10 $mA \cdot cm^{-2}$ below 575 mV which is ~100 mV lower than during dark mode. Additionally, it was proven that the accurate preparation of the TaS_2-based catalyst via sample centrifugation can significantly enhance the catalytic performance of the material. Solution-processed TaS_2-enabled PD exhibited broadband light sensitivity in the visible range. The highest photoresponsivity (0.68 $mA\ W^{-1}$) and specific detectivity (1.39 × 10^9 $cm\ Hz^{1/2}W^{-1}$) were observed under blue light illumination which was nearly double in comparison to green, red and far-red lights. These findings can potentially ignite multiple insights of $2H\text{-}TaS_2$ in the photo-induced electrochemistry and (nano)optoelectronics.

AUTHOR INFORMATION

Corresponding Author

Evgeniya Kovalska – Department of Inorganic Chemistry, University of Chemistry and Technology Prague, Technická 5, 166 28 Prague 6, Czech Republic; https://orcid.org/0000-0002-8996-0790. Email: evgeniya.kovalska.ua@gmail.com

Zdenek Sofer – Department of Inorganic Chemistry, University of Chemistry and Technology Prague, Technická 5, 166 28 Prague 6, Czech Republic; https://orcid.org/0000-0002-1391-4448. Email: soferz@vscht.cz

Authors

Pradip Kumar Roy – Department of Inorganic Chemistry, University of Chemistry and Technology Prague, Technická 5, 166 28 Prague 6, Czech Republic.

Nikolas Antonatos – Department of Inorganic Chemistry, University of Chemistry and Technology Prague, Technická 5, 166 28 Prague 6, Czech Republic.

Vlastimil Mazanek – Department of Inorganic Chemistry, University of Chemistry and Technology Prague, Technická 5, 166 28 Prague 6, Czech Republic.

Martin Vesely – Department of Organic Technology, University of Chemistry and Technology Prague, Technická 5, 166 28 Prague 6, Czech Republic.

Bing Wu – Department of Inorganic Chemistry, University of Chemistry and Technology Prague, Technická 5, 166 28 Prague 6, Czech Republic.

REFERENCES

1   Voiry, D. *et al.* Conducting MoS_2 Nanosheets as Catalysts for Hydrogen Evolution Reaction. *Nano Letters* **13**, 6222-6227, doi:10.1021/nl403661s (2013).

2   Voiry, D. *et al.* Enhanced catalytic activity in strained chemically exfoliated WS_2 nanosheets for hydrogen evolution. *Nature Materials* **12**, 850-855, doi:10.1038/nmat3700 (2013).

3   Li, Y., Li, Y.-L., Araujo, C. M., Luo, W. & Ahuja, R. Single-layer MoS_2 as an efficient photocatalyst. *Catalysis Science & Technology* **3**, 2214-2220, doi:10.1039/C3CY00207A (2013).

4   Bai, S., Wang, L., Chen, X., Du, J. & Xiong, Y. Chemically exfoliated metallic MoS_2 nanosheets: A promising supporting co-catalyst for enhancing the photocatalytic performance of TiO_2 nanocrystals. *Nano Research* **8**, 175-183 (2015).

5   Liu, Q. *et al.* Stable Metallic $1T-WS_2$ Nanoribbons Intercalated with Ammonia Ions: The Correlation between Structure and Electrical/Optical Properties. *Advanced Materials* **27**, 4837-4844, doi:10.1002/adma.201502134 (2015).

6   Tsai, C., Chan, K., Nørskov, J. K. & Abild-Pedersen, F. Theoretical insights into the hydrogen evolution activity of layered transition metal dichalcogenides. *Surface Science* **640**, 133-140, doi:https://doi.org/10.1016/j.susc.2015.01.019 (2015).

7   Johari, P. & Shenoy, V. B. Tuning the Electronic Properties of Semiconducting Transition Metal Dichalcogenides by Applying Mechanical Strains. *ACS Nano* **6**, 5449-5456, doi:10.1021/nn301320r (2012).

8   Chhowalla, M. *et al.* The chemistry of two-dimensional layered transition metal dichalcogenide nanosheets. *Nature chemistry* **5**, 263-275, doi:10.1038/nchem.1589 (2013).

9   Tan, C. & Zhang, H. Two-dimensional transition metal dichalcogenide nanosheet-based composites. *Chemical Society Reviews* **44**, 2713-2731, doi:10.1039/C4CS00182F (2015).

10   Chiritescu, C. *et al.* Ultralow thermal conductivity in disordered, layered WSe_2 crystals. *Science (New York, N.Y.)* **315**, 351-353, doi:10.1126/science.1136494 (2007).

11   Li, H. *et al.* Mechanical Exfoliation and Characterization of Single- and Few-Layer Nanosheets of WSe_2, TaS_2, and $TaSe_2$. *Small* **9**, 1974-1981, doi:10.1002/smll.201202919 (2013).

12   Peng, J.-P. *et al.* Molecular beam epitaxy growth and scanning tunneling microscopy study of $TiSe_2$ ultrathin films. *Physical Review B* **91**, 121113, doi:10.1103/PhysRevB.91.121113 (2015).

13   Wang, J. *et al.* Controlled Synthesis of Two-Dimensional 1T-TiSe2 with Charge Density Wave Transition by Chemical Vapor Transport. *Journal of the American Chemical Society* **138**, 16216-16219, doi:10.1021/jacs.6b10414 (2016).

14   Joe, Y. I. *et al.* Emergence of charge density wave domain walls above the superconducting dome in 1T-$TiSe_2$. *Nature Physics* **10**, 421-425, doi:10.1038/nphys2935 (2014).

15   Xi, X. *et al.* Strongly enhanced charge-density-wave order in monolayer $NbSe_2$. *Nature Nanotechnology* **10**, 765-769, doi:10.1038/nnano.2015.143 (2015).

16   Xi, X. *et al.* Ising pairing in superconducting $NbSe_2$ atomic layers. *Nature Physics* **12**, 139-143, doi:10.1038/nphys3538 (2016).

17   Sun, S. *et al.* Direct observation of an optically induced charge density wave transition in $TaSe_2$. *Physical Review B* **92**, 224303, doi:10.1103/PhysRevB.92.224303 (2015).

18   Yu, Y. *et al.* Gate-tunable phase transitions in thin flakes of 1T-TaS_2. *Nature Nanotechnology* **10**, 270-276, doi:10.1038/nnano.2014.323 (2015).

19   Hovden, R. *et al.* Atomic lattice disorder in charge-density-wave phases of exfoliated dichalcogenides (1T-TaS_2). *Proceedings of the National Academy of Sciences* **113**, 11420-11424, doi:10.1073/pnas.1606044113 (2016).

20   Sipos, B. *et al.* From Mott state to superconductivity in 1T-TaS$_2$. *Nature Materials* **7**, 960-965, doi:10.1038/nmat2318 (2008).

21   Tsen, A. W. *et al.* Structure and control of charge density waves in two-dimensional 1T-TaS$_2$. *Proceedings of the National Academy of Sciences* **112**, 15054, doi:10.1073/pnas.1512092112 (2015).

22   Pan, J. *et al.* Enhanced Superconductivity in Restacked TaS$_2$ Nanosheets. *Journal of the American Chemical Society* **139**, 4623-4626, doi:10.1021/jacs.7b00216 (2017).

23   Navarro-Moratalla, E. *et al.* Enhanced superconductivity in atomically thin TaS$_2$. *Nature Communications* **7**, 11043, doi:10.1038/ncomms11043 (2016).

24   Peng, J. *et al.* Disorder Enhanced Superconductivity toward TaS$_2$ Monolayer. *ACS Nano* **12**, 9461-9466, doi:10.1021/acsnano.8b04718 (2018).

25   Zong, P.-A. *et al.* Flexible Foil of Hybrid TaS$_2$/Organic Superlattice: Fabrication and Electrical Properties. *Small* **16**, 1901901, doi:10.1002/smll.201901901 (2020).

26   Wu, X.-C., Tao, Y.-R. & Gao, Q.-X. Fabrication of TaS$_2$ nanobelt arrays and their enhanced field-emission. *Chemical Communications*, 6008-6010, doi:10.1039/B913935D (2009).

27   Yoshida, M. *et al.* Controlling charge-density-wave states in nano-thick crystals of 1T-TaS$_2$. *Scientific Reports* **4**, 7302, doi:10.1038/srep07302 (2014).

28   Tsen, A. W. *et al.* Structure and control of charge density waves in two-dimensional 1T-TaS$_2$. *Proceedings of the National Academy of Sciences* **112**, 15054-15059, doi:10.1073/pnas.1512092112 (2015).

29   Hu, Y. *et al.* Toward Exploring the Structure of Monolayer to Few-layer TaS$_2$ by Efficient Ultrasound-free Exfoliation. *Nanoscale Research Letters* **13**, 20, doi:10.1186/s11671-018-2439-z (2018).

30   Nguyen, T. P. *et al.* Transition Metal Disulfide Nanosheets Synthesized by Facile Sonication Method for the Hydrogen Evolution Reaction. *The Journal of Physical Chemistry C* **120**, 3929-3935, doi:10.1021/acs.jpcc.5b12164 (2016).

31   Sutto, T. E. & Averill, B. A. in *Lower-Dimensional Systems and Molecular Electronics* (eds Robert M. Metzger, Peter Day, & George C. Papavassiliou) 289-291 (Springer US, 1990).

32 Zhou, L. *et al.* Tantalum disulfide quantum dots: preparation, structure, and properties. *Nanoscale Research Letters* **15**, 20, doi:10.1186/s11671-020-3250-1 (2020).

33 Kovalska, E. *et al.* Non-aqueous solution-processed phosphorene by controlled low-potential electrochemical exfoliation and thin film preparation. *Nanoscale* **12**, 2638-2647, doi:10.1039/c9nr10257d (2020).

34 Kovalska, E., Antonatos, N., Luxa, J. & Sofer, Z. "Top-down" Arsenene Production by Low-Potential Electrochemical Exfoliation. *Inorganic Chemistry* **59**, 11259-11265, doi:10.1021/acs.inorgchem.0c00243 (2020).

35 Kovalska, E. *et al.* Single-Step Synthesis of Platinoid-Decorated Phosphorene: Perspectives for Catalysis, Gas Sensing, and Energy Storage. *ACS Applied Materials & Interfaces*, doi:10.1021/acsami.0c15525 (2020).

36 Yin, H.-J., Zhou, J.-H. & Zhang, Y.-W. Shaping well-defined noble-metal-based nanostructures for fabricating high-performance electrocatalysts: advances and perspectives. *Inorganic Chemistry Frontiers* **6**, 2582-2618, doi:10.1039/C9QI00689C (2019).

37 Konanki, S. S. & Beyette, F. R. in *2000 Digest of the LEOS Summer Topical Meetings. Electronic-Enhanced Optics. Optical Sensing in Semiconductor Manufacturing. Electro-Optics in Space. Broadband Optical Networks (Cat. No.00TH8497).* I13-I14.

38 Sung, S. H., Schnitzer, N., Brown, L., Park, J. & Hovden, R. Stacking, strain, and twist in 2D materials quantified by 3D electron diffraction. *Physical Review Materials* **3**, 064003, doi:10.1103/PhysRevMaterials.3.064003 (2019).

39 Li, Y., Xiao, H., Zhou, P. & Cao, J. Electronic structures of twist-stacked 1T-TaS$_2$ bilayers. *Physics Letters A* **383**, 2302-2308, doi:https://doi.org/10.1016/j.physleta.2019.04.043 (2019).

40 Wang, X. H. *et al.* Antimonene: A Promising Candidate for SF$_6$ Decomposition Gas Sensors With High Sensitivity and High Stability. *IEEE Electron Device Letters* **41**, 1408-1411, doi:10.1109/LED.2020.3012693 (2020).

41   Wang, K. *et al.* Electrical control of charged carriers and excitons in atomically thin materials. *Nature Nanotechnology* **13**, 128-132, doi:10.1038/s41565-017-0030-x (2018).

42   Hirata, T. & Ohuchi, F. S. Temperature dependence of the Raman spectra of 1T-TaS$_2$. *Solid State Communications* **117**, 361, doi:10.1016/s0038-1098(00)00468-3 (2001).

43   Wu, D. *et al.* Ultrabroadband photosensitivity from visible to terahertz at room temperature. *J Science Advances* **4**, eaao3057, doi:10.1126/sciadv.aao3057 % (2018).

44   Luxa, J. *et al.* 2H→1T Phase Engineering of Layered Tantalum Disulfides in Electrocatalysis: Oxygen Reduction Reaction. **23**, 8082-8091, doi:10.1002/chem.201701494 (2017).

45   Yuan, Y.-P., Ruan, L.-W., Barber, J., Joachim Loo, S. C. & Xue, C. Hetero-nanostructured suspended photocatalysts for solar-to-fuel conversion. *Energy & Environmental Science* **7**, 3934-3951, doi:10.1039/C4EE02914C (2014).

46   Paul, K. K. *et al.* Strongly enhanced visible light photoelectrocatalytic hydrogen evolution reaction in an n-doped MoS$_2$/TiO$_2$(B) heterojunction by selective decoration of platinum nanoparticles at the MoS$_2$ edge sites. *Journal of Materials Chemistry A* **6**, 22681-22696, doi:10.1039/C8TA06783J (2018).

47   Lu, Y. *et al.* Hierarchical CdS/m-TiO$_2$/G ternary photocatalyst for highly active visible light-induced hydrogen production from water splitting with high stability. *Nano Energy* **47**, 8-17, doi:https://doi.org/10.1016/j.nanoen.2018.02.021 (2018).

48   Najafi, L. *et al.* TaS$_2$, TaSe$_2$, and Their Heterogeneous Films as Catalysts for the Hydrogen Evolution Reaction. *ACS Catalysis* **10**, 3313-3325, doi:10.1021/acscatal.9b03184 (2020).

49   Li, H. *et al.* Atomic-Sized Pores Enhanced Electrocatalysis of TaS$_2$ Nanosheets for Hydrogen Evolution. **28**, 8945-8949, doi:10.1002/adma.201602502 (2016).

50   Shi, J. *et al.* Two-dimensional metallic tantalum disulfide as a hydrogen evolution catalyst. *Nature Communications* **8**, 958, doi:10.1038/s41467-017-01089-z (2017).

51   Tong, T. *et al.* Sensitive and Ultrabroadband Phototransistor Based on Two-Dimensional Bi$_2$O$_2$Se Nanosheets. **29**, 1905806, doi:10.1002/adfm.201905806 (2019).

52   Wen, J. *et al.* Ultra-broadband self-powered reduced graphene oxide photodetectors with annealing temperature-dependent responsivity. *Carbon* **153**, 274-284, doi:https://doi.org/10.1016/j.carbon.2019.07.033 (2019).

53   Long, M. *et al.* Room temperature high-detectivity mid-infrared photodetectors based on black arsenic phosphorus. **3**, e1700589, doi:10.1126/sciadv.1700589 %J Science Advances (2017).

54   Bera, K. P. *et al.* Graphene Sandwich Stable Perovskite Quantum-Dot Light-Emissive Ultrasensitive and Ultrafast Broadband Vertical Phototransistors. *ACS Nano* **13**, 12540-12552, doi:10.1021/acsnano.9b03165 (2019).